J Digit Imaging (2013) 26:578–593
DOI 10.1007/s10278-012-9552-9

Adaptive Segmentation of Vertebral Bodies from Sagittal MR Images Based on Local Spatial Information and Gaussian Weighted Chi-Square Distance

Qian Zheng · Zhentai Lu · Qianjin Feng · Jianhua Ma · Wei Yang · Chao Chen · Wufan Chen

Published online: 13 November 2012
© Society for Imaging Informatics in Medicine 2012

Abstract We present a novel method for the automatic segmentation of the vertebral bodies from 2D sagittal magnetic resonance (MR) images of the spine. First, a new affinity matrix is constructed by incorporating neighboring information, which local intensity is considered to depict the image and overcome the noise effectively. Second, the Gaussian kernel function is to weight chi-square distance based on the neighboring information, which the vital spatial structure of the image is introduced to improve the accuracy of the segmentation task. Third, an adaptive local scaling parameter is utilized to facilitate the image segmentation and avoid the optimal configuration of controlling parameter manually. The encouraging results on the spinal MR images demonstrate the advantage of the proposed method over other methods in terms of both efficiency and robustness.

Keywords Segmentation · Spatial neighboring information · Gaussian weight · Chi-square distance · Local scaling

Introduction

Segmentation of anatomical structures and pathologies from magnetic resonance (MR) images is a fundamental problem, since the results play a crucial role in various medical evaluations, including measure tissue volumes, diagnosis, treatment planning, and surgical navigation. The segmentation of vertebral bodies in MR images is much challenging and complex due to the relatively variations in soft tissue contrast and artifacts like radio-frequency inhomogeneity.

Manual segmentation is time-consuming and varies from case to case, so automatic or semi-automatic segmentation of MR images is clinically desired. Up to now, many considerable segmentation approaches based on image gray level information have been proposed extensively, such as fuzzy clustering [1], statistical classification [2], active contour model (ACM) [3–7], active shape model (ASM) [8], and active appearance model (AAM) [9] methods. One of the most widely used fuzzy clustering algorithms is the fuzzy c-means (FCM) algorithm, which was first proposed by Dunn [10] and promoted as the general FCM clustering algorithm by Bezdek [11]. An image can be represented in various feature spaces, and the FCM algorithm classifies the image by grouping similar data points in the feature space into clusters. This clustering is achieved by iteratively minimizing a cost function that is dependent on the distance of the pixels to the cluster centers in the feature domain. In the segmentation based on the statistical classification, Markov random field (MRF)-based methods [12] are used to segment MR images due to their capability of coping with noise in images. The image is viewed as MRF and the observed intensity and the contextual information were combined to guide the classification under a Bayesian framework. However, due to the overlaps between object and nearby tissue in the image gray distribution, fuzzy clustering and statistical classification methods based on gray level information are susceptible to environmental noise and image inhomogeneity. ACM is another popular image segmentation technique. The basic idea of the ACM is to evolve a curve to fit the desired object boundary according to predefined cost function. ACM is sensitive to initial curve placement and easily falls into local minimum. To increase the robustness of the

Q. Zheng · Z. Lu (✉) · Q. Feng · J. Ma · W. Yang · W. Chen (✉)
School of Biomedical Engineering, Southern Medical University,
Guangzhou 510515, China
e-mail: luzhentai@163.com
e-mail: chenwf@fimmu.com

C. Chen
School of Traditional Chinese Medicine,
Southern Medical University,
Guangzhou 510515, China

ACM, ASM establish a statistical model of the shape of target object by introducing a training mechanism, and the shape is constrained in a learned shape space during the iterative shape deformation procedures. One disadvantage of ASM is that limited image information extracted around the shape landmarks can be used to guide the shape deformation, but all the other information, i.e., the image information of the regions far from landmarks, cannot be modeled in ASM. To overcome this problem, a combination model of the shape and image appearance is constructed in AAM. The shape constrains and the abundant image appearance information are available synchronously for AAM.

Notably, as graph-based method [13, 14], NCut [15], extensively used for nature image segmentation, has been applied in MR image segmentation [16]. NCut-based approaches mainly include two steps. First, a weighted graph is constructed, where nodes of the graph correspond to image pixels, and the weight of the edge reflects the similarity between two joined nodes. A graph can be represented by an affinity matrix. Second, the image segmentation is performed by solving the eigenvectors and eigenvalues of the affinity matrix. This step follows a partitioning criterion that maximizes the total similarity within groups and minimizes the total similarity between different groups. Using NCut-based approaches, an image is usually segmented into several distinct regions rather than the target and the background, and the pixels have high similarity within each region. Through NCut, an optimal solution can be calculated elaborately by solving the eigenvectors and eigenvalues of the weight matrix.

NCut is a very flexible segmentation framework where appropriate image feature extraction methods and similarity metrics can be selected according to the specific segmentation task. J. Gamio et al. [17] applied Ncut to segment MR T1-weighted sagittal images of the spine using windowed histograms of intensity [18] as the most promising features. Due to the usage of the simple statistical characteristics of local histogram, Gamio's algorithm is not a good choice for segmenting the images with same statistical characteristics of local histogram and low-contrast objects. As a typical example, Fig. 1a, b illustrates that two windowed patches (A and B) share the same statistical characteristics of local histogram. The difference of the synthetic patch *A* and patch *B* is obvious. Meanwhile, the corresponding histograms are same as shown in Fig. 1c, d. The results demonstrate that local statistic feature of the intensity value cannot depict an image boundary exactly because of the spatial information not taken into account. In other words, the analysis of the local histograms does not allow the segmentation method to accurately separate the vertebral bodies from rest of the spine by the presence of nearby structures of similar intensity.

In the current paper, we develop a new approach to automatically segment vertebral bodies from spinal MR images. Our methodology is novel in the following ways: To build a new affinity matrix for advanced image segmentation, we first use a cutoff window around each pixel and stack the gray values inside the window into a vector, which local intensity is introduced to depict the image exactly and help to distinguish different tissues. Second, considering the contribution of the nearby pixels to the centered pixel, we adopt the Gaussian kernel function to incorporate local spatial information, thus allowing the suppression of noise and improve the accuracy of the segmentation. Third, an adaptive local scaling parameter is used to refine the segmentation rather than a fixed scaling parameter to avoid the manually tuned parameter. Finally, the built affinity is introduced into the segmentation process by using a graph-based method to achieve the complete target. Extensively experiments show that the present approach can accurately and efficiently segment the vertebral bodies from MR images containing the vertebral body lesions.

The remaining of the paper is organized as follows: "Materials and Methods" section describes the image data, the built affinity matrix, and the present method. In "Results" section, the experiments setup and the evaluation results are presented. Finally, the conclusions are given in "Conclusions" section.

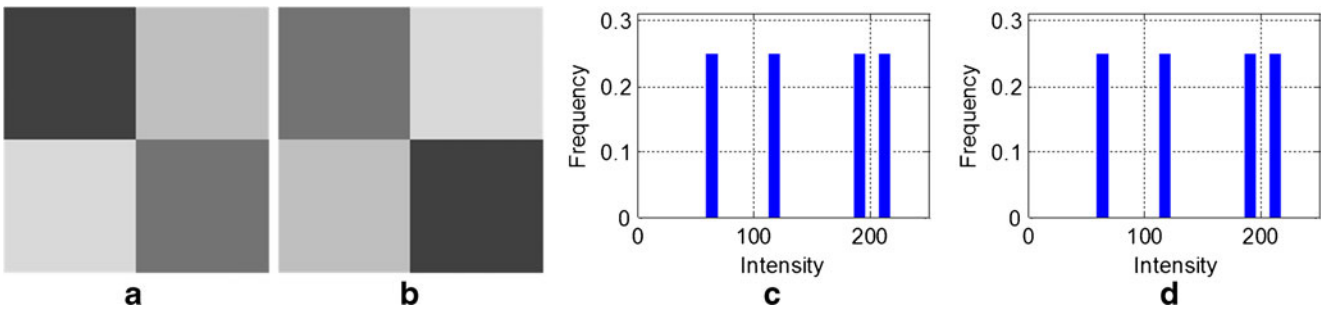

Fig. 1 Synthetic patches share the same statistical characteristic. **a** Patch *A*; **b** patch *B*. **c** The histogram of patch *A*; **d** the histogram of patch *B*

Materials and Methods

Image Data

Sagittal MR images of the spine were performed at 3.0 T with the protocol name of 8CTL L-SPINE/2, at the department of Orthopedics, Nanfang Hospital, Guangzhou, China and were collected from 2009 to 2010. The final data set comprised of 100 images (34 healthy and 66 unhealthy) of 40 patients. The patients' ages ranged from 40 to 65 years old. Patients were placed supine in the MR scanner, and T1-weighted and T2-weighted images were performed with the following parameters: pixel spacing=0.5859 mm, slice thickness=4 mm, image matrix size of 512 pixels×512 pixels, and slice spacing of 0.4 mm. A randomly selected 2D slice that was outlined by four independent trained radiologists with more than 20 years of clinical experience was considered the golden standard. Manual segmentations were performed using specially designed software and saved for validating the performance of the proposed method. The trained radiologist ensured that the segmented images covered the entire vertebral bodies.

Methodology

Graph-based image segmentation is an unsupervised segmentation method that casts image segmentation as a graph-partitioning problem. The given image I is represented as a weighted undirected graph $G=(V, E)$, with the pixels as graph nodes V and the connections between every pair of nodes as graph edge E. The above graph partitioning is based on the eigenvectors and eigenvalues of a $N\times N$ matrix derived from the matrix of pairwise affinities W. N represents the number of pixels in the image, and the weight of an edge is the measurement of the dissimilarity between the two pixels connected by that edge (e.g., the difference in brightness, distance, color, motion, location, or some other local attribute). The strength of these edges is weighted with an exponential factor and usually defined as

$$W_{ij} = e^{-\frac{d^2(i,j)}{\sigma^2}} \quad (1)$$

where $d(i, j)$ is the measure of the dissimilarity between pixels i and j and σ controls the scale of this measure.

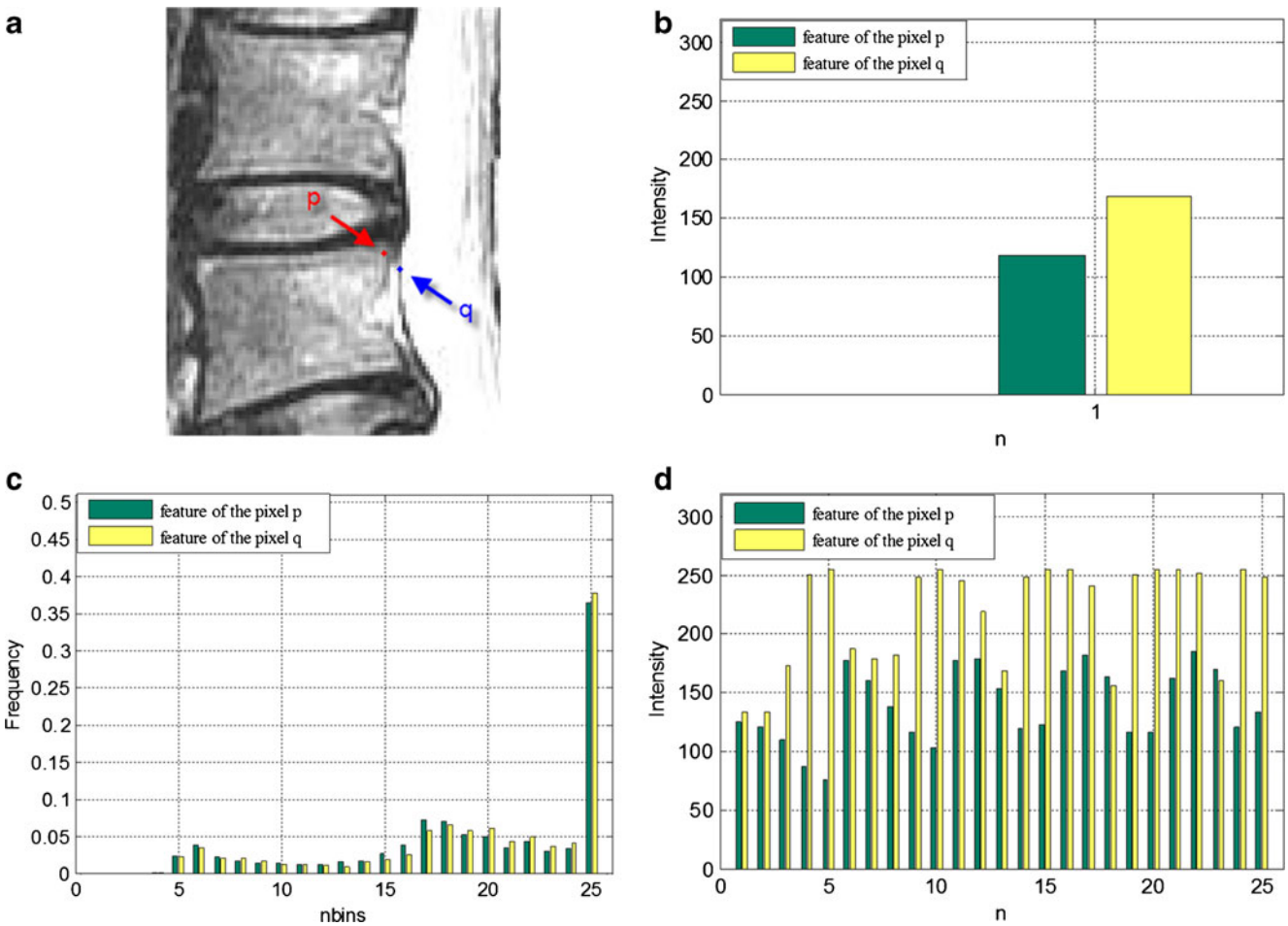

Fig. 2 Comparisons of the three used grey features. **a** The position of the pixel p and q; **b** the intensity of the p and $q(n=1)$; **c** the windowed histograms q(nbins=25); **d** the windowed intensities using our algorithm (n=25)

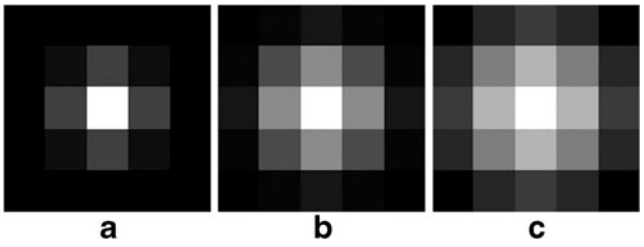

Fig. 3 The weights of the neighborhood. **a** l=0.5. **b** l=0.75. **c** l=1.0

Various Affinity Matrixes

We briefly introduce three affinity matrixes and compare them in "Results" section. A well-known example of an affinity matrix that uses intensity information is that NJW [19] algorithm, which is defined as

$$W_{ij} = e^{-\frac{\|I_i - I_j\|^2}{\sigma^2}} \tag{2}$$

where I_i and I_j denote the intensities of pixel i and pixel j, respectively. NJW algorithm is sensitive to noise and other imaging artifacts.

J Gamio et al. [17] proposed another new affinity matrix which uses local neighborhood information.

$$W_{ij} = e^{-\frac{\chi^2_{ij}}{\sigma^2}} \tag{3}$$

$$\chi^2_{ij} = \frac{1}{2}\sum_{k=1}^{nk}\frac{\left(h_i(k) - h_j(k)\right)^2}{h_i(k) + h_j(k)} \tag{4}$$

where h_i k is the number of pixels with intensity inside the range of the k-th bin of the i-th local histogram, i.e., the local histogram of the i-th pixel. This method will lead to poor segmentation because the various patches maybe share the same statistical characteristics.

Next, we consider a more complex matrix based on intensity and intervening contours, and this matrix is referred to as Shi's algorithm [20], which is shown as

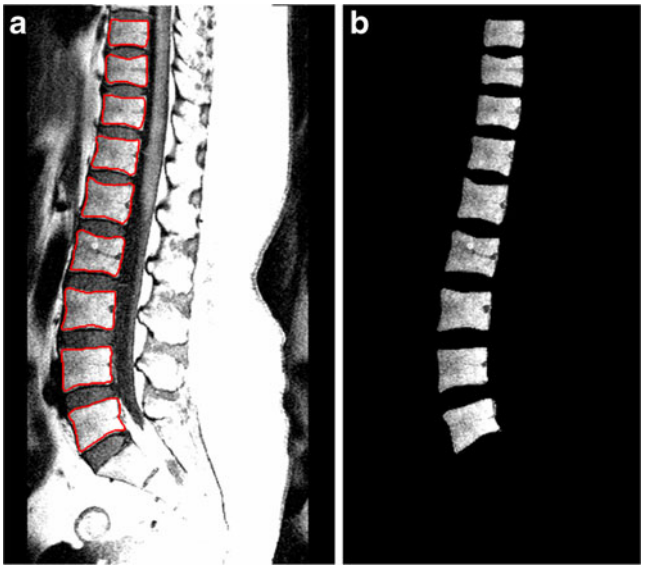

Fig. 5 Golden standard. **a** The boundaries of the vertebral bodies; **b** the segmented vertebral bodies

$$W_{ij} = \sqrt{W^I_{ij} \times W^C_{ij}} + \alpha W^C_{ij} \tag{5}$$

$$W^I_{ij} = e^{-\left\|X_i - X_j\right\|^2/\sigma_x - \left\|I_i - I_j\right\|^2/\sigma_I} \tag{6}$$

$$W^C_{ij} = e^{-\max_{x\in \mathrm{line(i,j)}}\|\mathrm{Edge(x)}\|^2/\sigma_C} \tag{7}$$

where X_i and I_i denote pixel location and intensity; line i, j is a straight line joining pixels i and j; Edge x is the edge strength at location x; σ_x, σ_I, and σ_C are the scale parameters; and α is the weight of the element $W_{ij}{}^C$. This approach has been found to be favor of image segmentation, but increase the parameters.

The overall quality of segmentation depends on the efficacious affinity matrix. In order to remedy the deficiency of the three approaches, we propose a novel affinity matrix that has a tendency to deliver good results in object segmentation.

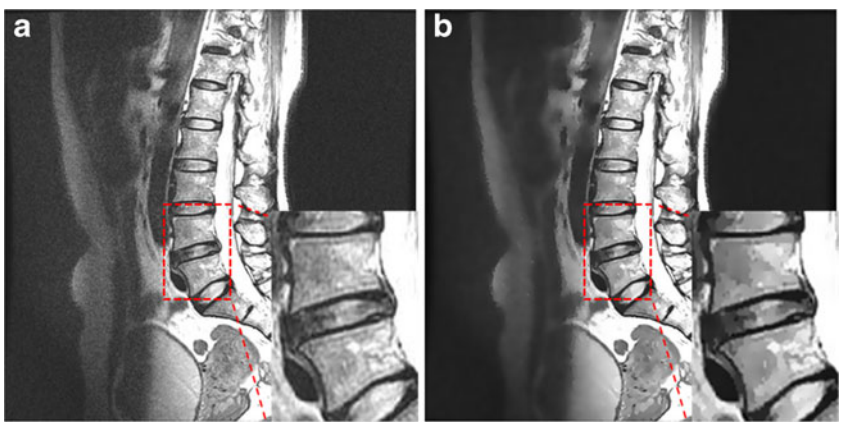

Fig. 4 The original and processed image. **a** The original image; **b** the processed image

Constructing the Novel Affinity Matrix

Local Spatial Neighbor Information and the Gaussian Weighted Chi-Square Distance

In NJW algorithm, only intensities information was used. However, the intensity varies significantly in certain tissues and organs because of the noise and artifacts. Moreover, the intensity of segmented object is close to the tissues growing around the object. J. Gamio et al. [17] used windowed histograms of intensity as the feature, thereby missing the spatial distribution information will result in incorrect results. One of the important characteristics of an image is that neighboring pixels are highly correlated. So we take into account the values of neighboring pixels to solve the above problem and extract a good spatial structure feature. A box of 5×5 pixels centered on each pixel is first used to extract local intensities of 25 pixels in order. Figure 2 shows the comparison between features, and the pixels p and q do not have the same intensity, as shown in Fig. 2b. Note that the difference between the histograms of p and q is very small (as shown in Fig. 2c), unlike the intensities of the local patch centered around the image pixels p and q (as shown in Fig. 2d).

The neighboring pixels possess similar feature values, and the probability that they belong to the same cluster is great. This spatial relationship is important in clustering. To introduce the spatial information in graph cut, a spatial function $h\ i$ is defined as

$$h(i) = \sum\nolimits_{k \in N_n} v_i(k) \tag{8}$$

where N_n denotes a local square neighborhood of the pixel i, n is the number of the square neighborhood of a fixed size, and $v_i\ k$ is the intensity of the k-th pixel of the local square neighborhood centered around the image pixel i. We incorporate the local

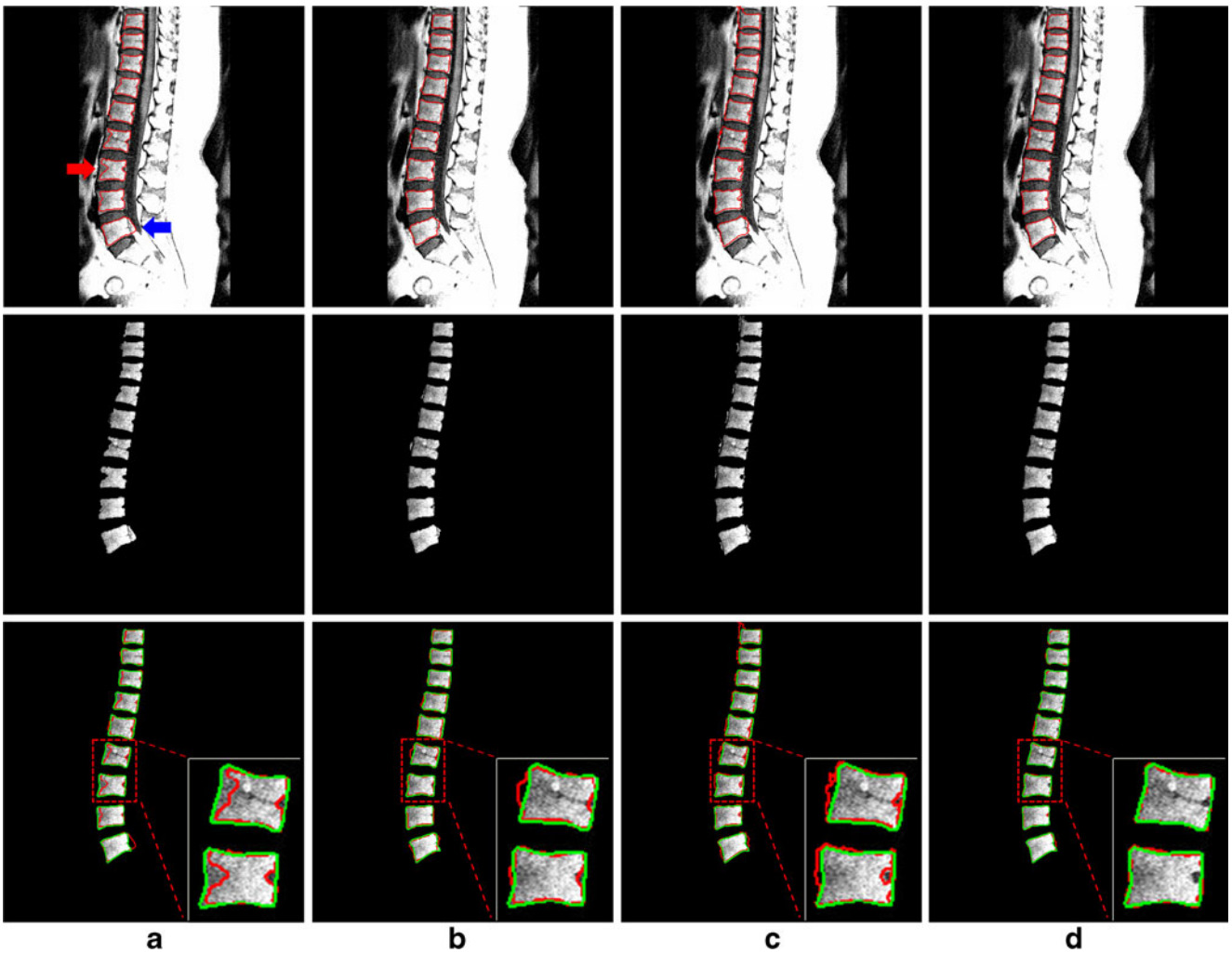

Fig. 6 Segmentation results by the various methods. **a** NJW algorithm (σ=0.2, C=35); **b** the Gamio's algorithm (σ=0.45, C=35); **c** the Shi's algorithm (σ_x=∞, σ_I=0.12, σ_C=0.08, α=1, C=65); **d** the present algorithm (C=40). **e** Golden standard. Row1 and row2 show the boundaries (*red line*) and segmentation results of the vertebral bodies, respectively. In row3, the golden standard is displayed in the *green line*, and the automatic segmentation is displayed in the *red line*

intensity and spatial information to the dissimilarity measure. The dissimilarity between a pair of pixels can be written as:

$$d^2(i,j) = \chi^2(h(i),h(j)) = \frac{1}{2}\sum_{k=1}^{n} w_k \frac{\left(v_i(k)-v_j(k)\right)^2}{v_i(k)+v_j(k)} \quad for \sum_{k=1}^{n} w_k = 1,\ w_k \geq 0 \tag{9}$$

where w_k is the feature weight of the k-th pixel. Weight w_k depends on the Euclidean distance between the center and the neighboring pixels. The closer the distance between the position of the neighboring and center pixel, the higher the weight value and vice versa.

$$w_k = G_l(p_i(k),p_i(i)) = \frac{1}{\sqrt{2\pi}l} e^{-\frac{\|p_i(k)-p_i(i)\|^2}{2l^2}} \tag{10}$$

where $p_i\ k$ is the spatial coordinate of the k-th pixel of the local square neighborhood centered around the image pixel i, and the parameter l controls the decay of the exponential function and the decay of the weights as a function of the Euclidean distances. Because the window size is 5×5, l should be between 0.5 and 1. To show the effect of the size l, the weights, coded in grayscale color map, of the neighborhood are shown in Fig. 3. The local intensities and spatial neighboring information are then combined and weighted through the Gaussian function. This affinity matrix not only considers the intensity of a single point but also the influence of neighboring pixels and the geometrical configuration in a whole neighborhood, which is incorporated to suppress the noise effectively and improve the accuracy of the segmentation.

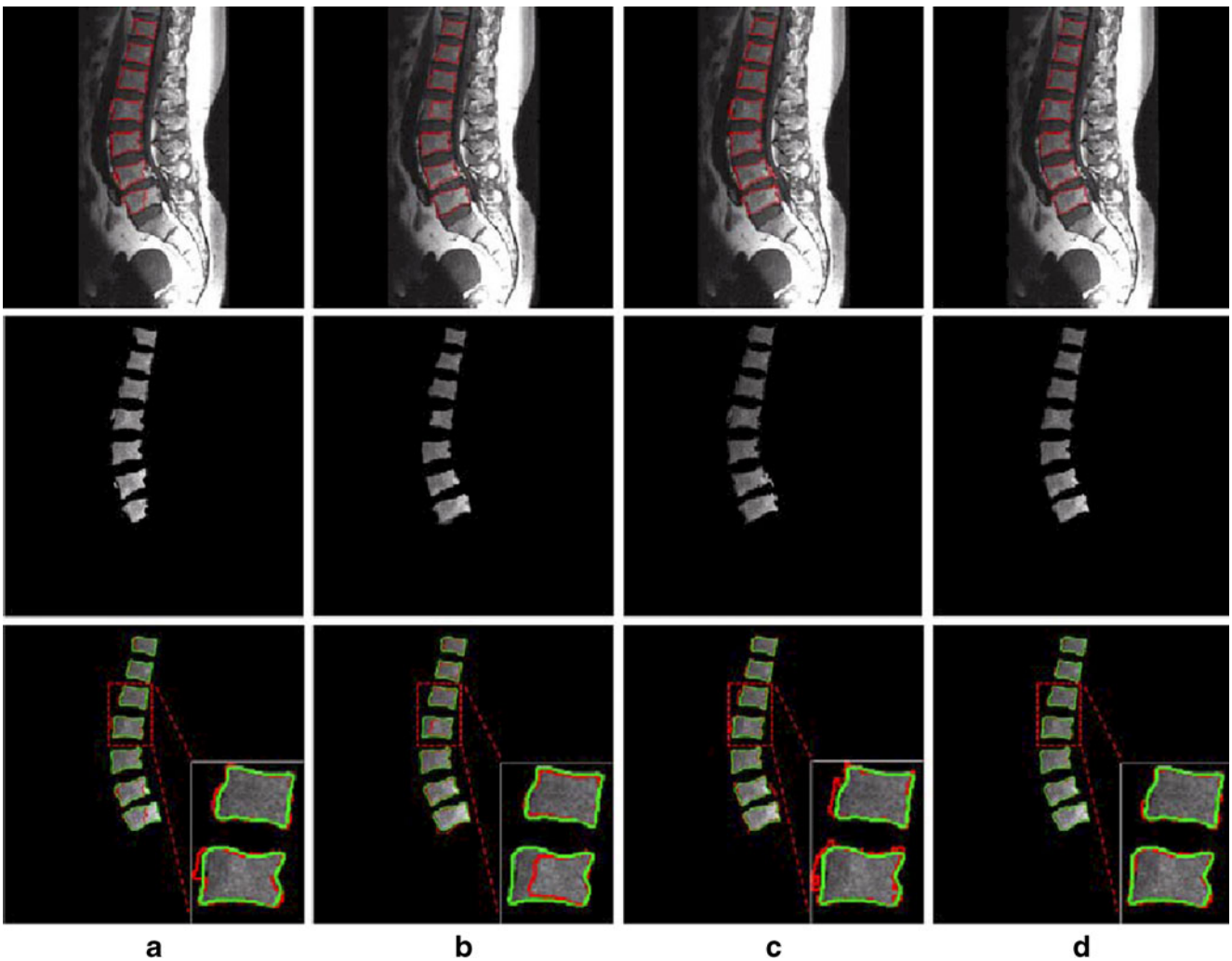

Fig. 7 Segmentation results by the various methods. **a** The NJW algorithm (σ=0.05, C=65); **b** the Gamio's algorithm (σ=0.15, C=40); **c** the Shi's algorithm (σ_x=∞, σ_I=0.02, σ_C=0.15, α=1, C=68); **d** the present algorithm (C=40). Row1 and row2 show the boundaries (*red line*) and segmentation results of the vertebral bodies, respectively. In row3, the golden standard is displayed in the *green line*, and the automatic segmentation is displayed in the *red line*

Local Scaling

The scaling parameter is used to control the similarity of two pixels. Andrew Y. Ng et al. ran their clustering algorithm repeatedly and selected σ from a number of values of σ using the criteria of least distorted clusters but the calculation cost is very expensive. The range of values to be tested should also be set manually. Rather than selecting a fixed scaling parameter σ, our approach aims to calculating a local scaling parameter σ_i for each pixel i, which is similar to the one proposed by Manor and Perona [21]. They used Euclidean distance between the two points, which is sensitive to the noise. In order to avoid the influence of the noise, we use the chi-square distance between the two points to incorporate the local spatial information. The distance from i to j as "seen" by i is $d\ i, j\ /\sigma_i$ while the converse is $d\ i, j\ /\sigma_j$. Therefore, the affinity between a pair of points can be given as:

$$W_{ij} = e^{-\frac{\chi^2(h(i),h(j))}{\sigma_i \sigma_j}} \tag{11}$$

$$\sigma_i == d(i,K) = \sqrt{\chi^2(h(i),h(K))} \tag{12}$$

The neighbors of pixel i are sorted in ascending order of the distance to i. Following the ordering process, pixel K is the K-th distant neighbor from point i. We choose a fixed and predetermined value of $K=7$, which gives good results even for various Gaussian window sizes. The adaptive local scaling is automatically computed to avoid the manually tuned parameter. The affinity should be large for pixels that should belong together and small if otherwise. With this adaptive local scaling, the present algorithm can remedy the deficiency of using a fixed scaling parameter and improve the segmentation results.

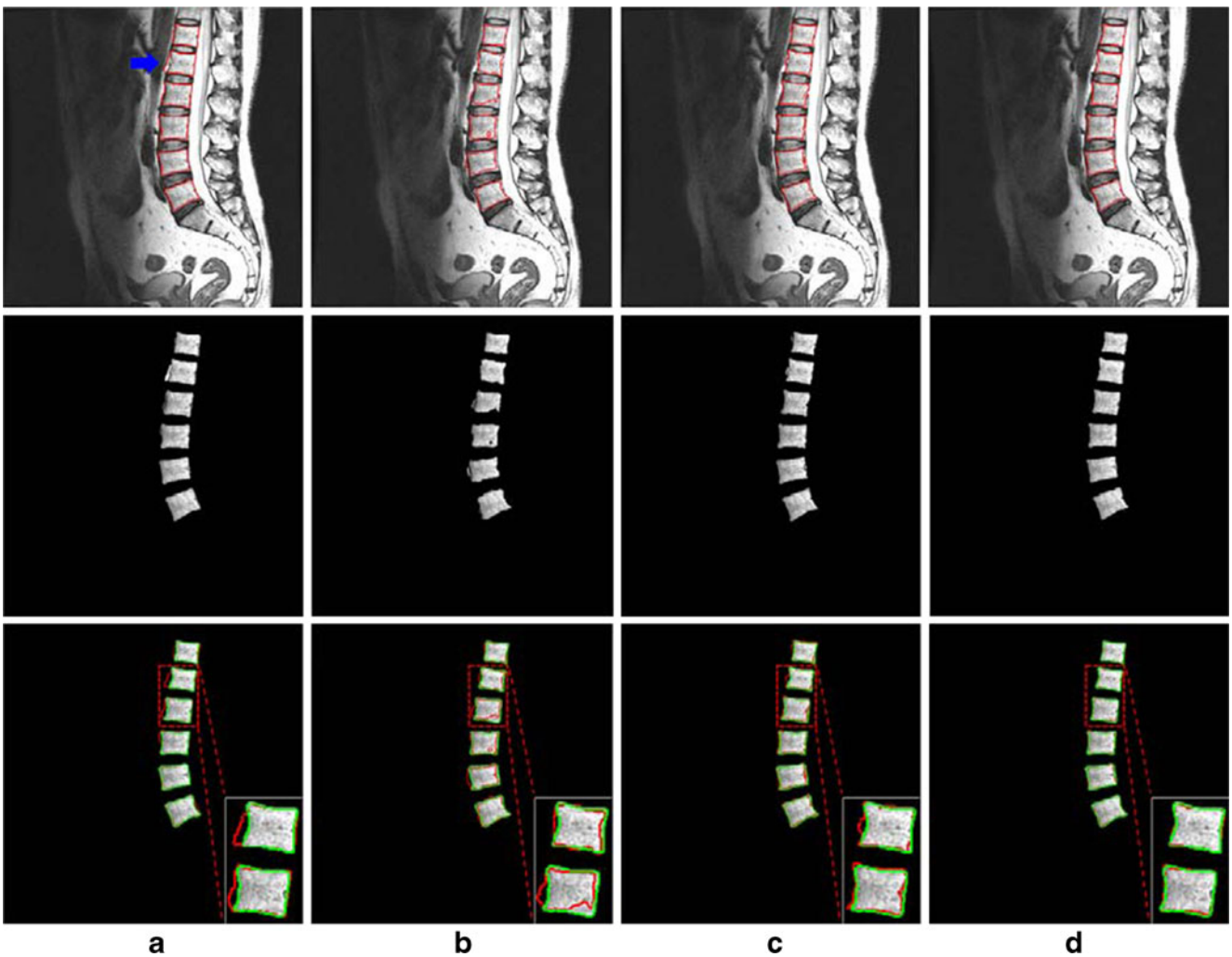

Fig. 8 Segmentation results by the various methods. **a** The NJW algorithm (σ=0.1, C=38); **b** the Gamio's algorithm (σ=0.12, C=40); **c** the Shi's algorithm (σ_x=∞, σ_I=0.2, σ_C=0.025, α=1, C=63); **d** the present algorithm (C=40); **e** golden standard. Row1 and row2 show the boundaries (*red line*) and segmentation results of the vertebral bodies, respectively. In row3, the golden standard is displayed in the *green line*, and the automatic segmentation is displayed in the *red line*

New Algorithm

Partitioning on the construction graph provides segmentation of the image regions by minimizing the cut functions, which play an important role in the process of segmentation. The common cut functions include minimum cuts [14], normalized cuts [15], and ratio cuts [22]. To find a balanced partition, we use the normalized cuts to segment the image and the objective function of our method is defined as

$$\Gamma(A_1,\ldots,A_C)=\frac{1}{2}\sum_{c=1}^{C}\frac{W\left(A_c,A_c\right)}{vol(A_c)},(A_1\cup A_2\ldots\cup A_C=I,A_1\cap A_2\ldots\cap A_C=\Phi) \quad (13)$$

$$W\left(A_c,\overline{A}_c\right)=\sum_{i\in A_c,j\in\overline{A}_c}W_{ij} \quad (14)$$

$$\mathrm{vol}(\mathrm{A_c})=\sum_{\mathrm{i}\in\mathrm{A_c}}\mathrm{d_i} \quad (15)$$

$$d_i=\sum_{j=1}^{N}W_{ij} \quad (16)$$

where A represents the set of all pixel nodes and I denotes the image, which is assumed to be portioned into C not necessarily disjoint sets $A_1, A_2, \ldots$ and A_c. $\overline{A}_c$ is the complement of A_c.

We use fixed choices C=40 and l=0.5 to obtain the segmentation of the vertebral bodies. We summarize our suggested algorithm as follows:

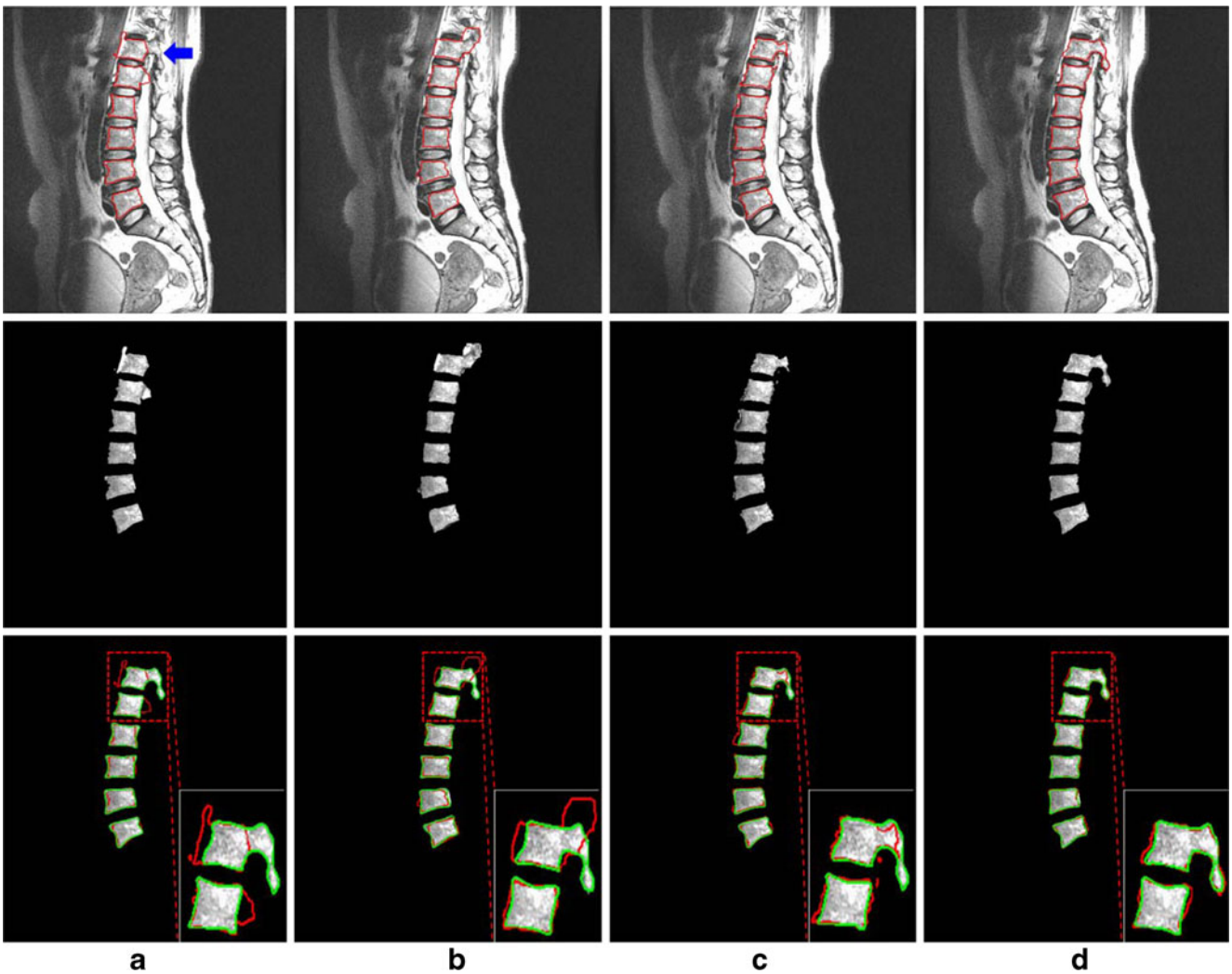

Fig. 9 Segmentation results by the various methods. **a** The NJW algorithm (σ=0.18, C=40); **b** the Gamio's algorithm (σ=0.35, C=35); **c** the Shi's algorithm ($\sigma_x=\infty$, σ_I=0.12, σ_C=0.12, α=1, C=70); **d** the present algorithm (C=40). Row1 and row2 show the boundaries (*red line*) and segmentation results of the vertebral bodies, respectively. In row3, the golden standard is displayed in the *green line*, and the automatic segmentation is displayed in the *red line*

1. Compute the dissimilarity and the local scale σ_i using Eqs. (9) and (12), respectively.
2. Form the locally scaled affinity matrix $W \in \Re^{N\times N}$ where W_{ij} is defined according to Eq. (11) for $i \neq j$ and $W_{ii}=0$.
3. Define D to be a diagonal matrix with $D_{ii} = \sum_{j=1}^{N} W_{ij}$ and construct the Laplacian matrix $L=D^{-1/2}WD^{-1/2}$.
4. Find $x_1,\cdots, x_C$, the C largest eigenvectors of L and form the matrix $X=[x_1,\cdots, x_C] \in \Re^{N\times C}$.
5. Re-normalize the rows of X to determine the unit length yielding $Y \in \Re^{N\times C}$, such that $Y_{ij} = X_{ij}/\left(\sum_j W_{ij}^2\right)^{1/2}$.
6. Treat each row of Y as a point in $\Re^C$ and cluster via k-means.
7. Assign the original point i to cluster c if and only if the corresponding row i of the matrix Y was assigned to cluster c.
8. Display the segmented vertebral bodies through the use of morphological operation.

Results

Comparison with Other Matrixes

In "Materials and Methods" section, we introduced three matrixes and constructed our novel matrix. The purpose of the experiments is to demonstrate that the algorithm using the novel matrix can improve the performance of the segmentation. All segmentations are done in a computer with an Intel Core Duo processor, 2.53 GHz, and 2 GB RAM. The original MR images are preprocessed by the anisotropic diffusion [23, 24] for the present method, the NJW, Shi's, and the Gamio's algorithms. Then, we give an example to exhibit the result after performing the anisotropic diffusion step, as shown in Fig. 4.

We divided the MR images of the patients in four categories: T1-weighted normal spine, T1 weighted with vertebral

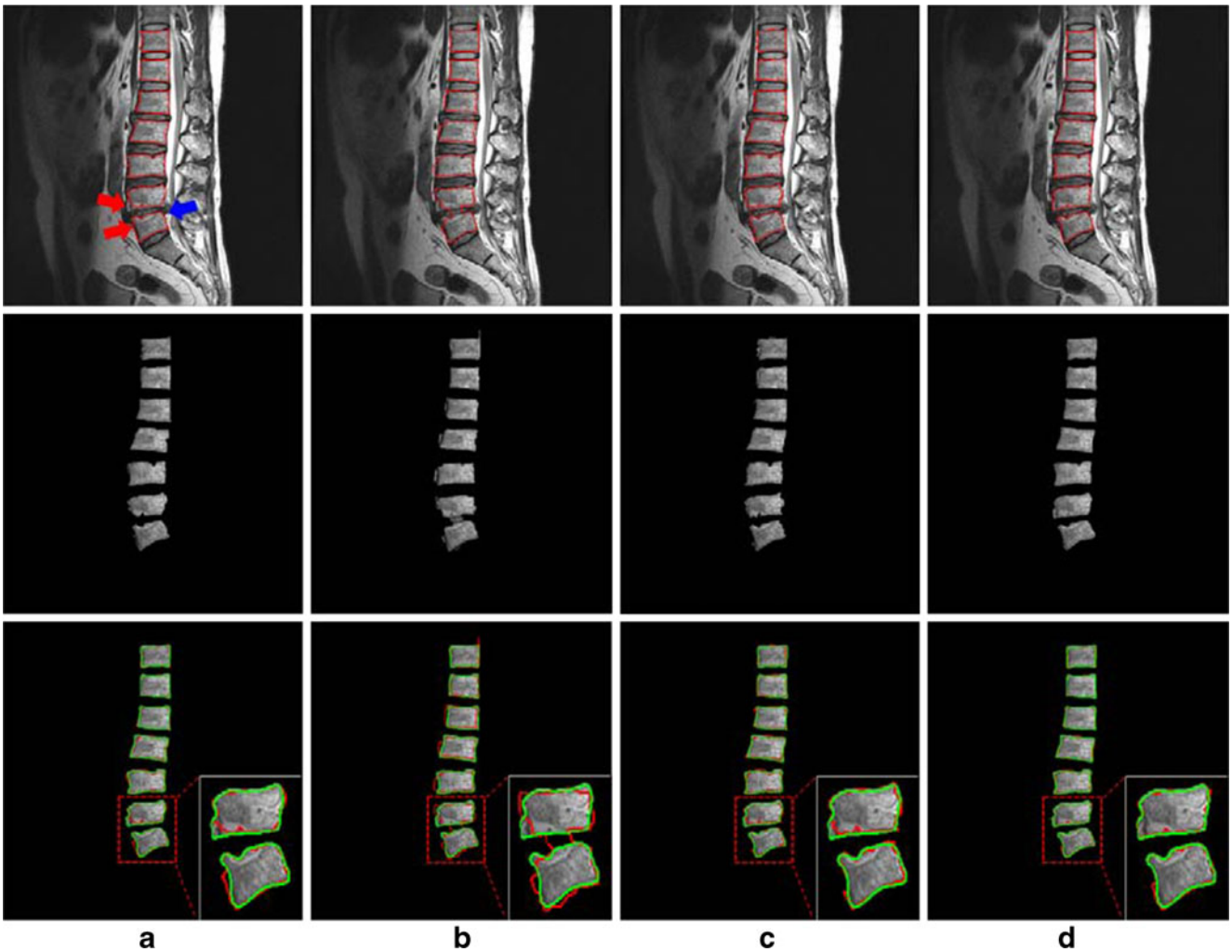

Fig. 10 Segmentation results by the various methods. **a** The NJW algorithm (σ=0.1, C=50); **b** the Gamio's algorithm (σ=0.1, C=40); **c** the Shi's algorithm ($\sigma_x=\infty$, σ_I=0.22, σ_C=0.05, α=1, C=90); **d** the present algorithm (C=40). Row1 and row2 show the boundaries (*red line*) and segmentation results of the vertebral bodies, respectively. In row3, the golden standard is displayed in the *green line*, and the automatic segmentation is displayed in the *red line*

Table 1 The comparisons between the four algorithms

Algorithm	Fig	Dice	ME	HD
NJW algorithm	5	0.901617	0.008217	3.3
	8	0.912605	0.006710	4.5
	11	0.947509	0.004051	1.7
	14	0.886505	0.008152	4.2
	17	0.957979	0.004467	1.7
Gamio's algorithm	5	0.92693	0.006344	2
	8	0.894051	0.007881	2
	11	0.891325	0.007866	1.7
	14	0.860596	0.010296	2.8
	17	0.902853	0.010391	2.2
Shi's algorithm	5	0.912966	0.007805	2.2
	8	0.929405	0.005768	2.8
	11	0.930789	0.005188	1.7
	14	0.913751	0.006432	3.5
	17	0.940525	0.006306	1.8
Improved algorithm	5	0.964549	0.003132	2
	8	0.964315	0.002842	1.7
	11	0.969118	0.002293	1.4
	14	0.962901	0.002724	1.7
	17	0.970673	0.003147	1.7

lesion and disk degeneration, T2-weighted normal spine, and T2-weighted with vertebral lesion and disk degeneration. T1-weighted scans work well for differentiating fat from water with water appearing darker and fat brighter. These scans are obtained to observe the anatomical structure of the spine. T2-weighted scans are another basic type. Like the T1-weighted scan, fat is differentiated from water—but in this case, fat shows darker and water lighter. In the case of spinal study, the cerebrospinal fluid will be lighter in T2-weighted images. These scans are acquired to examine the pathologic change of the spine.

Subject 1 T1-weighted normal spine

Figure 5 shows the result obtained by one of the four medical experts manually. The result is regarded as the golden standard, which is used to validate the feasibility and superiority of the algorithm. From Fig. 6, the NJW method is most likely to lead to the phenomena of under-segmentation (results are larger than the manual labels) in the joint location (refer to the blue arrow in Fig. 6a) which shows little contrast between vertebral bodies and the rest of the anatomical structures. Moreover, the pixel intensity in the same tissue varies sharply because of the noise and anisotropic factors, and NJW technique tends to over-segment in some vertebral bodies (refer to the red arrow in Fig. 6a).

The Gamio's algorithm uses the windowed histograms of intensity as the most promising features, but the histograms do not consider the spatial information. It can be seen from the Fig. 6b that the vertebral bodies are segmented in accordance with the object boundaries. However, it uses a single scaling parameter, which must be tuned for the optimal result manually. In Fig. 6c, the segmentation results of the vertebral bodies we obtain by the Shi's algorithm is not smooth due to the information of intervening contours.

The present method uses local scaling and takes into account the intensity of each pixel as well as the intensity of the neighboring pixels. This approach to the self-acting segmentation of vertebral bodies has encouraging results on the location of the intensities of the vertebral bodies, which are similar to the tissues around the vertebral bodies. Obviously, the phenomena of over-segmentation and under-segmentation can then be reduced effectively. The vertebral bodies are cleanly separated from the spine using the local spatial information, as shown in Fig. 6d.

Subject 2 The patient has vertebral body lesions and disk degeneration (T1-weighted)

The patients suffer from vertebral disease, such as degenerative spondylosis and spinal disk herniation. Figure 7 shows the encouraging results of the present method. In this experiment, the proposed metric allows the segmentation

Table 2 The comparisons between the four algorithms

Method	Parameter					Time (s)
	Intensity information	Position information	Intervene contours	The weight	Cluster number	
NJW	$\surd(\sigma)$	×	×	×	$\surd(C)$	51.47
Gamio's	$\surd(\sigma)$	×	×	×	$\surd(C)$	53.29
Shi's	$\surd(\sigma_I)$	$\surd(\sigma_x)$	$\surd(\sigma_C)$	$\surd(\alpha)$	$\surd(C)$	15.25
Improved	×	×	×	×	$\surd(C)$	57.01

The √ denotes the method has the parameter, if not is ×

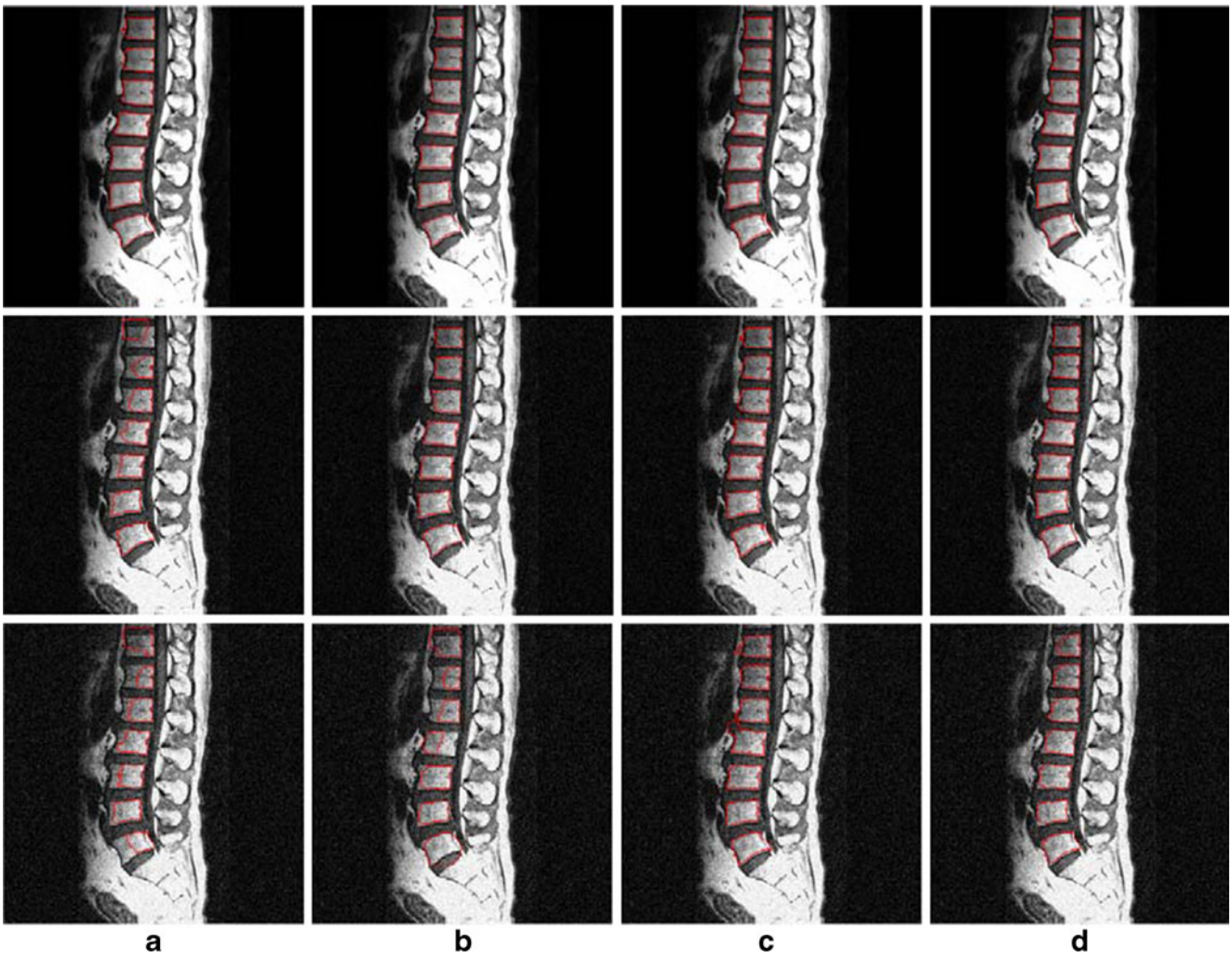

Fig. 11 Comparisons of the four algorithms on segmentation results with zero-mean Gaussian white noise. **a** The NJW algorithm; **b** the Gamio's algorithm; **c** the Shi's algorithm; **d** the present algorithm. *Row1* the original image and the segmentation results; *row2* the image which is added Gaussian white noise with variances 0.01 and the segmentation results; *row3* the image which is added Gaussian white noise with variances 0.02 and the segmentation results

technique to accurately separate the degenerative vertebral bodies from the rest of the thoracic image despite its weak edge and the presence of nearby structures of similar intensity. It can be seen that the NJW algorithm, Gamio's algorithm, and Shi's algorithm cannot find the desired object boundary exactly, but the improved approach resulted in fewer pixels being misclassified.

Subject 3 T2-weighted normal

The vertebral bodies of the patient are normal in the 2D sagittal magnetic resonance images of the spine, and the vertebral bodies show high contrast with respect to the intervertebral bodies and surrounding structures. The vertebral bodies are easier to segment compared with other images. Figure 8 shows how the NJW algorithm leads to a few of the phenomena in under-segmentation (refer to the blue arrow in Fig. 8). The segmentation of vertebral bodies by the Gamio's algorithm is much smaller than the golden standard. The improved algorithm segments the vertebral bodies smoothly, clearly, and accurately. The segmented boundary of the present method is very close to the golden standard. We can observe from Fig. 8a–c that the NJW algorithm, the Gamio's algorithm, and the Shi's algorithm fail to segment the object, while the correct segmentation result is obtained from the present method.

Then, we consider the Fig. 9. Here, the vertebral bodies of the patient are normal, and the pedicle of vertebral arch is scanned because of the different scanning flip angles. As we all know, the pedicle of vertebral arch is a part of the vertebral body so we should segment the pedicle of vertebral arch together with the vertebral body. The new algorithm is capable of extending further to segment the

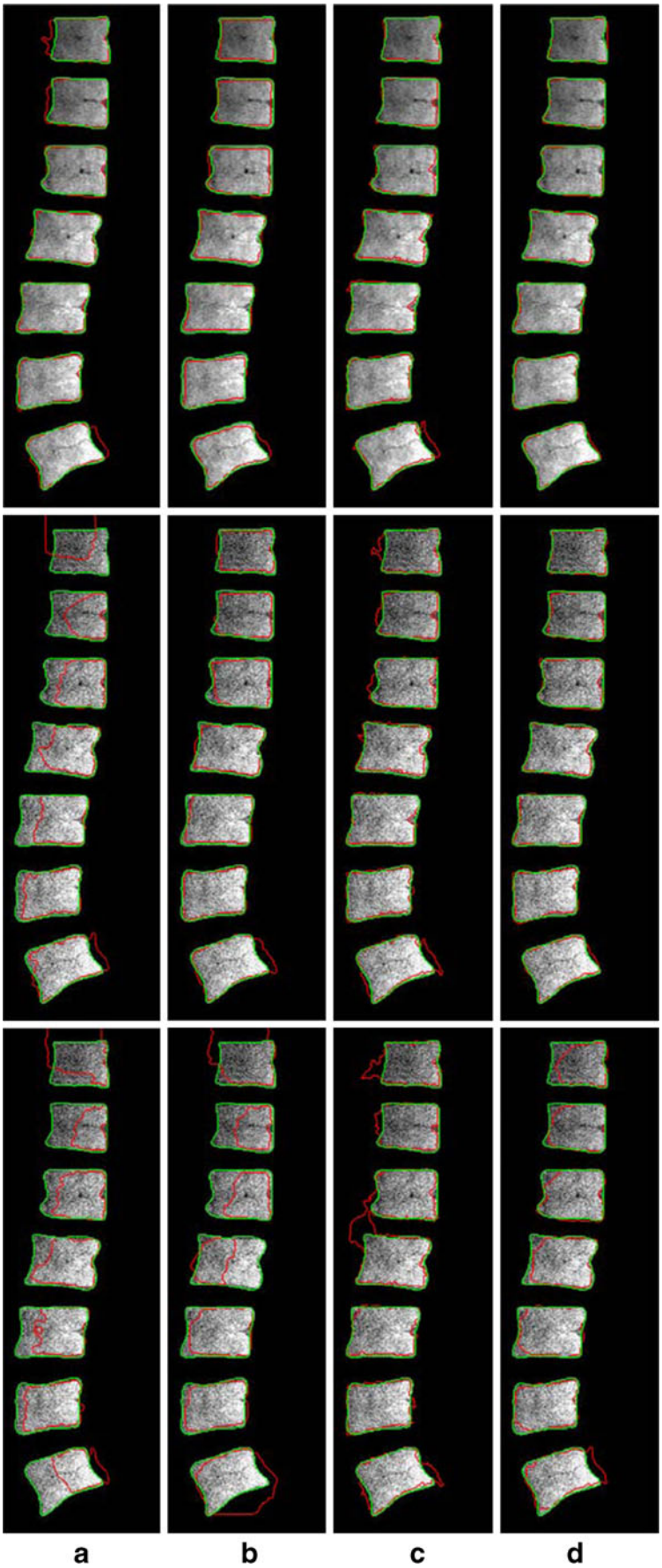

Fig. 12 Zoom portions of the segmentation results. The golden standard is displayed in the *green line*, and the automatic segmentation is displayed in the *red line*. **a** The NJW algorithm; **b** the Gamio's algorithm; **c** the Shi's algorithm; **d** the present algorithm. *Row1* the original image; *rows 2* and *3* are added Gaussian white noise with variances 0.01 and 0.02, respectively

pedicle of vertebral arch (refer to the blue arrow in Fig. 9). The Gamio's algorithm performed well in the vertebral bodies showing high contrast with respect to the intervertebral disks and surrounding structures (as shown in Fig. 9). However, the performance was poor if the condition was not satisfied (as shown in Figs. 7 and 9). This improved algorithm can segment the vertebral bodies smoothly, clearly, and accurately. The segmented results of the improved algorithm are more similar to the golden standard than those of NJW algorithm, Shi's algorithm, and Gamio's algorithm.

Subject 4 The patient has vertebral body lesions and disk degeneration (T2-weighted)

One will have vertebral body lesions (refer to the red arrow in Fig. 10) and disk degeneration (refer to blue the arrow in Fig. 10) with advancing age. There is bright prospect in the vertebral bodies via the limitation of imaging methods, which increases the level of complexity in the image. Consequently, the segmented result of the NJW algorithm is very poor, as illustrated in Fig. 10. Again, a clear improvement is shown. Although the patient has vertebral body lesions and disk degeneration, the segmentation of the present algorithm is much more accurate than the other algorithms.

Dice index [25], misclassification error (ME) [26], and Hausdorff distance (HD) [27] are selected to evaluate the accuracy of segmentation. The Dice, ME, and HD are, respectively, given by

$$\mathrm{Dice} = \frac{2 \times |\mathrm{F_{Manual}} \cap \mathrm{F_{Auto}}|}{|\mathrm{F_{Manual}}| + |\mathrm{F_{Auto}}|} \tag{17}$$

$$\mathrm{ME} = 1 - \frac{|\mathrm{B_{Manual}} \cap \mathrm{B_{Auto}}| + |\mathrm{F_{Manual}} \cap \mathrm{F_{Auto}}|}{|\mathrm{B_{Manual}}| + |\mathrm{F_{Manual}}|} \tag{18}$$

$$\mathrm{HD}(\mathrm{F_{Manual}}, \mathrm{F_{Auto}}) = \max[\mathrm{h}(\mathrm{F_{Manual}}, \mathrm{F_{Auto}}), \mathrm{h}(\mathrm{F_{Auto}}, \mathrm{F_{Manual}})] \tag{19}$$

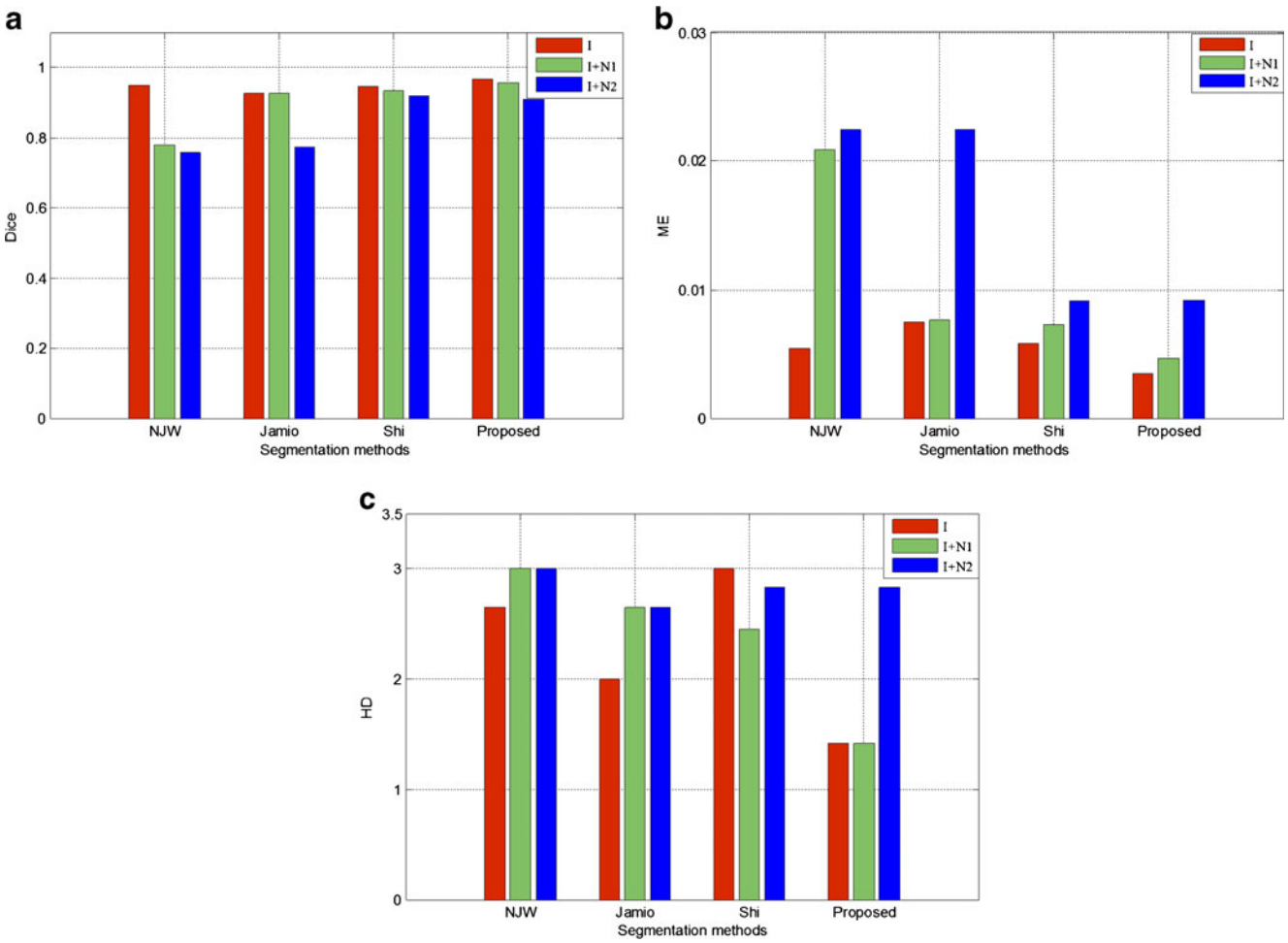

Fig. 13 Dice, ME, and HD similarity measures computed for all methods. Original image is shown in *red*, and the images added Gaussian white noise with variances 0.01 and 0.02 are shown in *green* and *blue*, respectively

where F_{Manual} and B_{Manual} are the foreground and background of the manual algorithm, respectively, as the F_{Auto} and B_{Auto} are foreground and background of the automatic algorithm, and the $|F_{\text{Manual}}|$ denotes the number of pixels assigned to the foreground by the medical expert. Dice index measures the similarity between automatic segmentation results and the golden standard, whereas ME measures error ratio between automatic segmentation results and the golden standard. The higher the value of Dice index, the better the overall performance of the segmentation will be. Dice index equal to 1 suggests a good match between manual and automatic segmentation. The lower the ME ratio, the fewer the misclassified pixels are. HD measures the maximum distance between two contours. According to Table 1, the segmentation results of the present approach are much more accurate than the other algorithms.

The Comparison of the Variability

The NJW algorithm and the Gamio's algorithm segment the objects base on the intensity information. So in the segmentation process, the parameter of the intensity information must be set and tuned manually. The Shi's algorithm based on intensity and intervening contours increases the scaling parameter parameters and the complexity. We incorporate the spatial information to the present segmentation algorithm by introducing the adaptive local scaling to avoid the manually tuned scaling parameter σ repeatedly. In many cases, there is no appropriate scaling parameter to obtain the good segmentation results. Comparison of the manually tuned parameters is as in Table 2, and the parameters, which are set at the beginning of the experiments and need not tune, do not listed, such as the nbins of the Gamio's method.

Our algorithm has the least parameter than other methods, in which the parameters σ, σ_I, σ_x, σ_C, α, and C have high impact on the segmentation quality. The parameters selected manually from a number of values, and this requires a significant calculation, which is expensive. The range of values to be tested should also be set manually. We repeat abundant number of experiment and choose the best ones for the NJW, the Gamio's, and the Shi's algorithms by experts. In our method, the Gaussian weighted local spatial information and adaptive scaling parameter σ_i for each pixel i makes the set of cluster number easier to set parameter C, as shown in Figs. 6, 7, 8, 9, and 10. Here, we can utilize the fixed parameter C(=40) to obtain the high-quality segmentation results.

The execution time for the present method, the NJW, Shi's, and the Gamio's algorithms are shown as in Table 2, and the cost times of the computation of the affinity matrix are 0.3366, 0.3571, 0.6864, and 0.7650 s, respectively. Although the proposed algorithm took more time than other methods, it is just a calculation unlike other methods due to the optimal configuration of controlling parameter manually.

Sensitivity to Noise

To study the effect of noise on the performance, a real image is added zero-mean Gaussian white noise, and the segmentation results are shown in Figs. 11 and 12. The original image and the segmentation results are shown in row1. Rows 2 and 3 in Fig. 11 show the segmentation results on

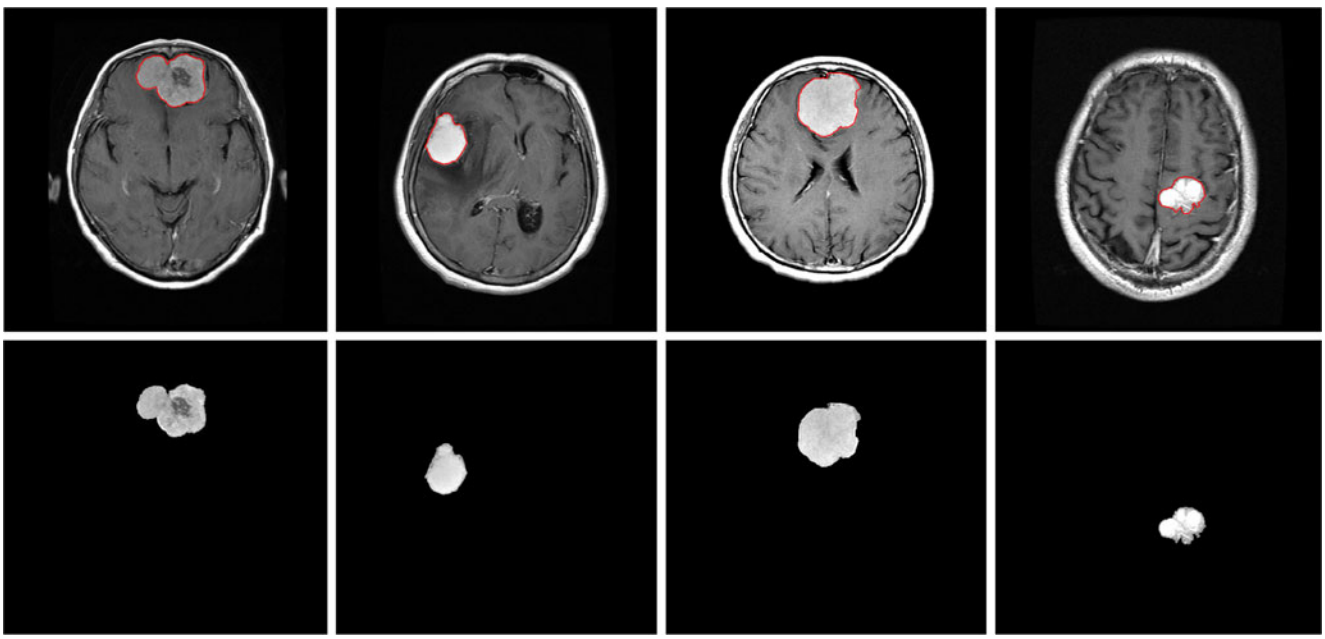

Fig. 14 The segmentations of the meningioma of four patients (window size=7×7,C=6). *Top row* the boundary of the segmented meningioma; *bottom row* the segmentation results of the meningioma

image added zero-mean Gaussian white noise with variances 0.01 and 0.02, respectively. We show in Fig. 13 the Dice, ME, and HD similarity measures for the whole segmentation, in the four methods studied, and in order to compare, we show in Fig. 13 the Dice, ME, and HD values, scaled to a range of the various and appropriate size. In both sub-images, the ordering of the methods is: the NJW algorithm, the Gamio's algorithm, the Shi's algorithm, and the present algorithm. From Figs. 11, 12, and 13, we can see that the proposed algorithm has higher anti-noise for the Gaussian noise.

The encouraging results with real MR images demonstrate the superior performance of the present method over other clustering methods in terms of both accuracy and robustness. The present method is a general one which can be devoted to developing segmentation of other tissues and organs. According to Fig. 14, the edge of the meningioma is not smooth, but our algorithm can obtain the object boundary correctly. All segmentations are done in a computer with an Intel Core Duo processor, 2.53 GHz, and 2 GB RAM.

Conclusions

In this work, we present an adaptive segmentation algorithm using local spatial neighboring information and Gaussian weighted chi-square distance. In the traditional algorithms, the parameter setting requires labor-intensive and time-consuming. We incorporate the weighted spatial structure information into the affinity matrix to allow for the affinity between two pixels to be influenced by their neighborhoods, which not only improve the accuracy of segmentation results but also overcome the noise effectively. Additionally, the scale parameters can be tuned automatically. The experimental results show that the proposed method has stronger anti-noise property and higher segmentation precision than other matrixes. The robust and accurate result of segmentation should serve image registration and the analysis of spinal deformities. It can also be used in organ location and image-guided vertebra operation, with presumed significant clinical impact.

The future work is to differentiate the normal vertebral bodies from the unmoral vertebral bodies and estimate vertebral fracture risk evaluation by using of the segmentation results. Furthermore, as a reviewer's comment, for decreasing the computational time, a localization method like the generalized Hough transform will be a interspersing choice to improve the efficiency of the algorithm and meet the real-time requirements, instead of processing the entire image and utilizing the GPU or the multi-scale graph decomposition.

Acknowledgments The authors gratefully acknowledge the useful comments and suggestions of the editors and reviewers, which have improved this manuscript. This work is partially supported by the National Science Foundation of China (project no. 31000450, no. 81000613) and the Major State Basic Research Development Program of China (973 Program, no. 2010CB732500).

References

1. Gath I, Geva AB: Unsupervised optimal fuzzy clustering. IEEE Transportation Pattern Analytical Machine Intelligence 11:773–781, 1989
2. Schillo C, Herrmann G, Ackermann F, et al: Statistical classification and segmentation of biomolecular surfaces. Proceedings International Conference Image Processing 3(3):560–563, 1995
3. Kass M, Witkin A, Terzopoulos D: Snakes: Active contour models. International J Computer Vision 5:321–331, 1988
4. Caselles V, Kimmel R, Sapiro G: Geodesic active contours. International J Computer Vision 22(1):61–79, 1997
5. Ronfard R: Region-based strategies for active contour models. International J Computer Vision 46:223–247, 2002
6. Paragios N, Deriche R: Geodesic active contours and level sets for detection and tracking of moving objects. IEEE Transaction Pattern Analysis Machine Intelligence 22:1–15, 2000
7. Chan T, Vese L: Active contour without edges. IEEE Transaction Image Processing 10(2):266–277, 2001
8. Cootes TF, Taylor CJ, Cooper DH, Graham J: Active shape models —their training and application. Computer Vision Image Understanding (61) 38–59, 1995
9. Mitchell SC, Bosch JG, Lelieveldt BP, et al: 3-d active appearance models: segmentation of cardiac MR and ultrasound images. IEEE Transport Medicine Imaging 21(9):1167–1178, 2002
10. Dunn JC: A fuzzy relative of the ISODATA process and its use in detecting compact well separated cluster. J Cybernet 3(3):32–57, 1974
11. Bezdek JC: Pattern recognition with fuzzy objective function algorithms. Kluwer Academic, Norwell, 1981
12. J, Gray RM: Image Segmentation and Compression Using Hidden Markov Models (Monograph). Norwell: Kluwer Academic, 2000
13. Greig DM, Porteous BT, Seheult AH: Exact maximum a posteriori estimation for binary images. J Royal Statistical Society Series B 51:271–279, 1989
14. Wu Z, Leahy R: An optimal graph theoretic approach to data clustering: theory and its application to image segmentation. IEEE Transactions Pattern Analysis Machine Intelligence 15(11):1101–1113, 1993
15. Shi J, Malik J: Normalized cuts and image segmentation. IEEE Transactions Pattern Analysis Machine Intelligence 22(8):888–905, 2000
16. Angayarkanni P: MRI mammogram image segmentation using ncut method and genetic algorithm with partial filters. IJCSI International J Computer Science Issues 8(1):455–459, 2011
17. Gamio J, Belongie S, Majumdar S: Normalized cuts in 3D for spinal MRI segmentation. IEEE Transactions Medical Imaging 23 (1):36–44, 2004
18. Malik J, Belongie S, Leung T, et al: Contour and texture analysis for image segmentation. International J Computer Vision 43(1):7–27, 2001
19. Ng A, Jordan M, Weiss Y: On spectral clustering: analysis and an algorithm. Advances Neural Information Processing Systems (NIPS) 849–856, 2001
20. Cour T, Benezit F, Shi J: Spectral segmentation with multiscale graph decomposition. IEEE Conference Computer Vision Pattern Recognition 2(2):1124–1131, 2005

21. Zelnik ML, Perona P: Self-tuning spectral clustering. Advances Neural Information Processing Systems (NIPS) 1601–1608, 2004
22. Hagen L, Kahng A: New spectral methods for ratio cut partitioning and clustering. IEEE Transactions Computer-Aided Design 11 (9):1074–1085, 1992
23. Perona P, Malik J: Scale-space and edge detection using anisotropic diffusion. IEEE Transportation Pattern Analytical Machine Intelligence 12:629–639, 1990
24. Perona P, Shiota T, Malik J: Anisotropic diffusion. Geometry-Driven Diffusion Computer Vision 1:73–92, 1994
25. Mayer A, Greenspan H: An adaptive mean-shift framework for MRI brain segmentation. IEEE Transactions Image Processing 28 (8):1238–1250, 2009
26. Sezgin M, Sankur B: Survey over image thresholding techniques and quantitative performance evaluation. J Electronic Imaging 13 (1):146–165, 2004
27. Alt H, Guibas LJ: Discrete geometric shapes: matching, interpolation, and approximation. In: Sack JR, Urrutia J Eds. Handbook of Computational Geometry. Amsterdam: Elsevier Science, 2000, pp 121–153